Korean J. Chem. Eng., **31**(8), 1306-1315 (2014)
DOI: 10.1007/s11814-014-0136-x
pISSN: 0256-1115
eISSN: 1975-7220

REVIEW PAPER

Surface forces apparatus and its applications for nanomechanics of underwater adhesives

Dongyeop Xris Oh*, Sara Shin, Hee Young Yoo***, Chanoong Lim****, and Dong Soo Hwang*,**,***,****,†**

*POSTECH Ocean Science and Technology Institute, Pohang University of Science and Technology (POSTECH), Pohang 790-784, Korea
**School of Environmental Science and Engineering, Pohang University of Science and Technology (POSTECH), Pohang 790-784, Korea
***Integrative Biosciences and Biotechnology, Pohang University of Science and Technology (POSTECH), Pohang 790-784, Korea
****School of Interdisciplinary Bioscience and Bioengineering, Pohang University of Science and Technology (POSTECH), Pohang 790-784, Korea
(*Received 25 February 2014 • accepted 8 May 2014*)

Abstract−Successful adhesion on wet surfaces is one of the most important challenges in biomedical engineering. Marine fouling organisms exhibit effective adhesion for wet substrates, and the measurement of adhesion forces in wet conditions is the first step toward mimicking the smart strategies of the marine organisms. Surface forces apparatus (SFA) is one of the most powerful nanomechanical tools used to directly measure time- and distance-dependent interactions between biological macromolecules or biological surfaces in an aqueous medium at the molecular level. Recently, SFA has been adapted to probe the biomechanical nature of the underwater adhesive in marine organisms. This review describes some strategies of the marine fouling organisms for successful underwater adhesion determined using SFA.

Keywords: Surface Forces Apparatus, L-3,4-Dihydroxyphenyl Alanine (DOPA), Underwater Adhesion, Complex Coacervate, Cation-π Interaction, Marine Adhesive, Underwater Adhesion

INTRODUCTION

Adhesives are indispensable because most products, ranging from low-tech applications (e.g., books, pencils, and boxes) to high-tech applications (e.g., electric devices, medical devices, automobiles, and airplanes), generally contain at least one adhesive material [1]. Since the advent of synthetic adhesives in the early 20th century, much progress has been made in the adhesive technology. This includes the pressure-sensitive adhesive (PSA) on the Post-it note and ceramic tile adhesive for space shuttles that can endure extreme heat and stress [2]. Despite such impressive progress, adhesives that work in wet conditions have not yet been developed because water molecules generally reduce the bonding abilities of adhesive molecules [3]. However, the demand for specialized adhesives for wet surfaces is steadily increasing, particularly in the medical field where most surfaces are hydrated. Moreover, underwater adhesives can replace rigid medical wound closures such as stitches, screws, metal pins, and plates, which can delay tissue recovery and induce secondary tissue damages [4]. Therefore, the development of underwater adhesive is a challenging yet important task for many biomedical applications [5].

Some key insights and principles in designing underwater bioadhesives have been found in marine fouling organisms (e.g., marine algae, mussels, tubeworms, barnacles, hydroids, octopus eggs, and sea stars) [6-11] (Fig. 1). Marine fouling organisms secrete specialized adhesives to attach themselves to wet and rough marine substratum to protect themselves against biological, chemical, and mechanical stresses from the ocean. Indeed, bioadhesives from marine fouling organisms have fascinating properties such as robust wet adhesion, good adhesion to different types of substrates, biocompatibility, and environmental friendliness [12-15]. To date, biochemical studies on the bioadhesives of mussels and sandcastle worms have suggested three key mechanisms for successful underwater adhesion: 1) L-3,4-dihydroxyphenylalanine (DOPA) chemistry, 2) cation-π interactions, and 3) complex coacervation (Fig. 2).

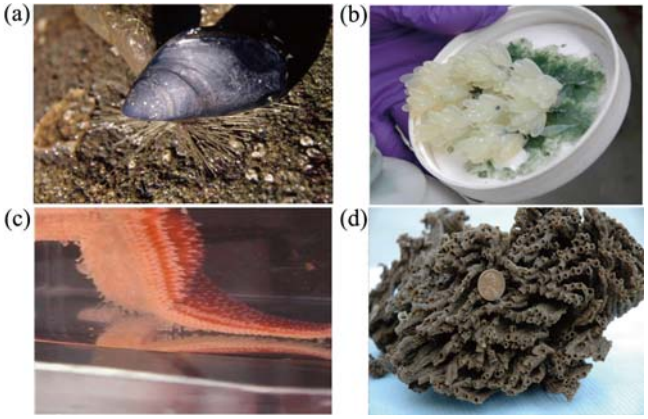

Fig. 1. Marine fouling organisms: (a) a mussel and its byssus, (b) eggs of the octopus, (c) a sea star, and (d) sandcastle built by a sandcastle worm. Fig. 1(a) was kindly provided by Dr. Minho Son (Marine Eco-Technology Institute) and Fig. 1(d) was provided by Dr. ChengJun Sun (First Institute of Oceanography, China).

†To whom correspondence should be addressed.
E-mail: dshwang@postech.ac.kr

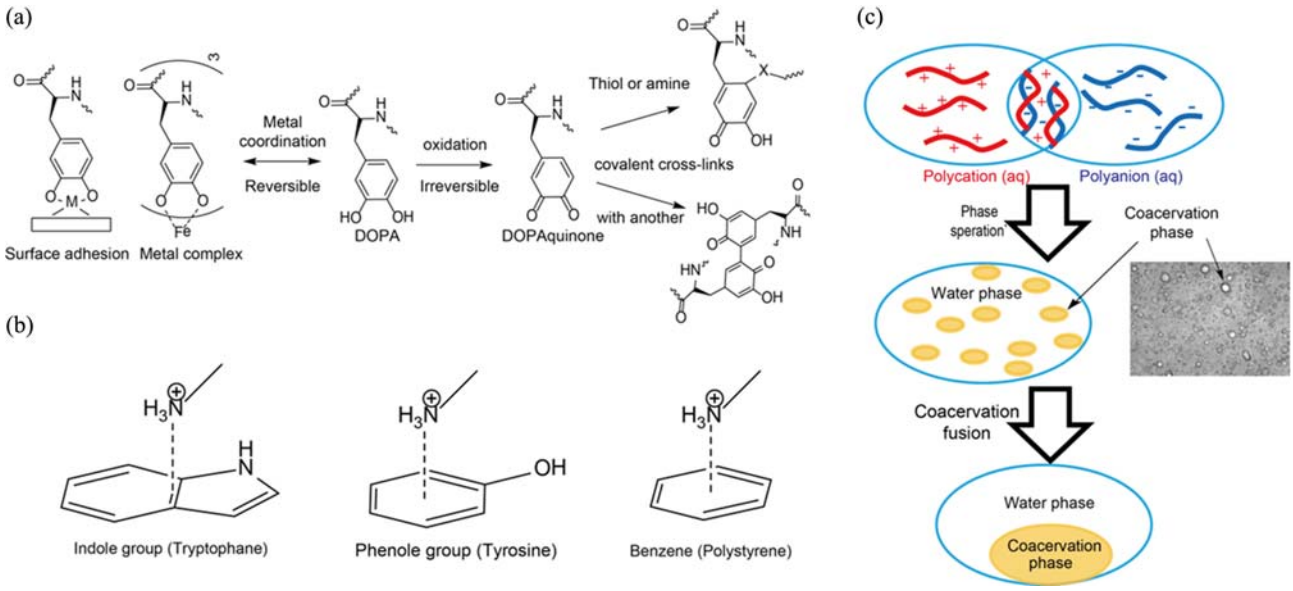

Fig. 2. Three key mechanisms for underwater adhesion: (a) DOPA chemistry, (b) cation-π interaction, and (c) complex coacervation.

First, the underwater adhesion processes of marine fouling organisms, including mussels and sandcastle worms, (Figs. 1(a) and 1(d)) are commonly mediated by DOPA, a catecholic amino acid [16-19] (Fig. 2(a)). DOPA mediates underwater adhesion via two strategies: 1) the intact DOPA groups in adhesive proteins form a reversible chelation with the surface metal oxide or 2) the oxidized DOPA groups in adhesive proteins permanently (covalently) couple with thiols, amines, or other catechols [17]. The metal chelation not only provides a strong adhesion onto substratum surfaces (interfacial stickiness between the adhesive protein and substratum), but also provides a reversible/self-healing property to the adhesive unit after high deformation [16,18]. Moreover, the oxidative covalent coupling of DOPA in the mussel byssus matrix increases cohesion (mutual stickiness in bulk) strength [19].

Second, cation-π interactions, which are present between the face of an electron-rich π system and an adjacent cation, have been considered as another key mechanism for robust noncovalent interactions in aqueous systems [20,21]. Because of their relatively high binding energy in aqueous systems, cation-π interactions play an important role in biological activities involving ion channels, molecular recognition, and molecular reception [22]. Recently, it has been revealed that cation-π interactions contribute to the underwater adhesion by mussel. Because mussel foot proteins (mfp), conventionally known as mussel adhesive proteins, are rich in cationic (Lys, His, Arg) and aromatic (Tyr, DOPA, His, and Trp) residues, they could contribute to cation-π interactions for successful underwater adhesion [23-25].

Third, marine fouling organisms utilize complex coacervation methods to concentrate adhesive materials into a condensed liquid phase and deliver them onto the target surfaces [26-29] (Fig. 2(c)). Two oppositely charged polyelectrolytes in aqueous solution at a specific pH range and ionic strength undergo a fluid-fluid phase separation into two phases—a dense phase with most of the polyelectrolytes and a polyelectrolyte-depleted equilibrium phase. The dense phase is called the "coacervate," and the entire process is referred to as "complex coacervation." Interestingly, the highly concentrated coacervate phase does not easily disperse into the water phase and has low interfacial energy to engulf the surrounding liquid or solid. Thus, the adhesives secreted from marine fouling organisms as a coacervate could readily infiltrate to the microholes on the target surface and spread out in high concentration and with minimal loss of the adhesive components.

Although these three key strategies have already been suggested by several valuable biochemical studies of marine bioadhesives, it is still a great challenge to develop a synthetic underwater adhesive because of the lack of understanding in the intermolecular interactions of the marine adhesive biopolymers in aqueous systems. Thus, understanding the adhesion phenomena of the underwater adhesive molecules at a molecular level is a vital prerequisite for the development of useful underwater adhesives. Several nanomechanical studies have been reported for the three key strategies [14,16,23-25,30]. In recent years, the nanomechanical measurements of underwater adhesion with regards to the three key mechanisms, (DOPA chemistry, cation-π interactions, and complex coacervation) have been actively performed using a surface forces apparatus (SFA). In this review, the recent advances in understanding the intermolecular interactions in marine adhesives, with regards to the three key insights, by using SFA, are summarized.

1-1. Surface Forces Apparatus (SFA)

The first SFA was developed by Tabor and Winterton in 1969 and later improved by Israelachvili and his coworkers in 1972. Israelachivili and Adams also designed the SFA technique for intermolecular force measurements in liquids [30]. SFA is now a representative and powerful instrument used to characterize the fundamental adhesive forces such as electrostatic forces, van der Waals forces, capillary forces, hydrophobic interactions, bio-specific interactions, metal coordination forces as well as friction force in wet conditions.

Atomic force microscope (AFM), developed by Binnig, Quate and Gerber, has also been extensively used to measure intermolecular forces in liquids [31,32]. However, it is difficult for AFM to

measure forces applied to highly deformable surfaces, soft materials such as polymer and biological surfaces, or highly repulsive surfaces because the absolute distance measurement between the tip and the surface of AFM has low reliability [33]. More specifically, in direct measurement of the distance between the AFM cantilever and the target surface via laser reflection, constant vibration of AFM cantilever during the measurement, surface deformation during the contact, and strong repulsive forces between the cantilever and the surface, make the absolute distance measurement difficult. However, SFA can precisely measures the forces as a function of the absolute distance between two surfaces due to the fringes of equal chromatic order (FECO) technology, which is further described in Section 2.2.1. Indeed, SFA can measure forces with ~1 nN sensitivity and less than 1 Å distance resolution. For more details, see the recent reviews on SFA [30].

SFA 2000, the latest SFA version from the Israelachvili research group, has been designed to facilitate manipulation and provide more diverse modulations for interfacial, tribological and rheological experiments [30,34]. Here we briefly describe the SFA setup, specifically for the SFA 2000 model. A schematic view of SFA setup for normal force measurements and illustration of a typical force-distance profile is shown in Fig. 3. SFA for normal adhesion force measurement consists of the set of micrometers, the central single-cantilever spring, the lower disk holder and the upper disk holder.

1-1-1. The Distance Control

The SFA 2000 has four levels of controls to manipulate the distance between the two opposing surfaces with 1 Å distance resolution. The specifications of these controls for the SFA 2000 are described in Table 1 and the SFA 2000 manual [30]. The bottom surface can be manipulated by three levels of control: fine, medium and coarse. The bottom surface moves by a central single-cantilever spring, which can generate both coarse and fine motions. The medium and the coarse levels can be manipulated by hand using the differential micrometer. The fine control is connected to a motor that drives the fine micrometer. These three different levels of control result in various movements of the bottom surface, which is equipped on the lower disk holder. For the movement of the top surface, there is an extra fine control on a piezoelectric tube. This extra fine control offers distance control with Ångstrom-level accuracy.

1-1-2. Adhesion Forces Measurement

The key elements in measuring the adhesion forces in the SFA are the spring constant of the cantilever spring on the bottom surface and its associated distance using Hook's law [35] (Fig. 3). The bottom surface is linked to the attachment base under the main stage through a double-cantilever force spring. The spring constant (k) hinges onto the spring selected by the desired force order and the distance between the two opposing surfaces (ΔD) resolves to within 0.1 nm using the optical interferometry image. ΔD is measured by multiple beam interferometry (MBI), which results from multiple light reflections between both surfaces. Optically transparent mica sheets are placed on both of the surfaces, on which various molecules could be coated. The outer opposing sides of the micas are typically coated

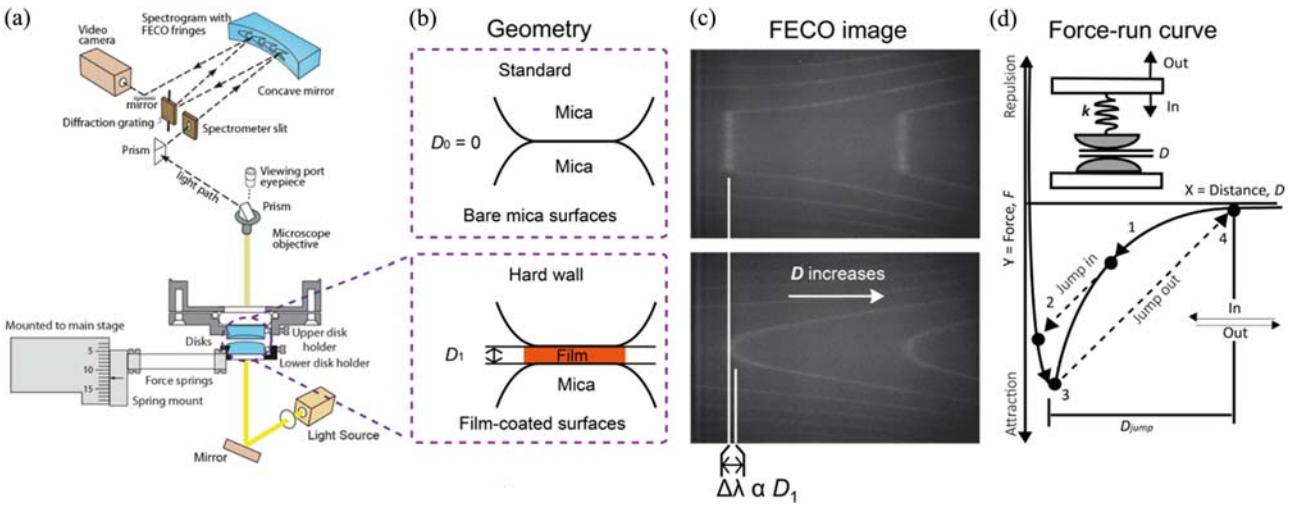

Fig. 3. The SFA experimental setup for normal force measurement. (a) Schematic view of the SFA instrument. (b) Two bare mica surfaces, (top) in flat contact and two film-coated surfaces, (bottom) in contact with a hard wall distance D. (c) The corresponding fringes of FECO images. (d) Illustration of a typical force-distance profile (force run), "jump in" denotes the attraction of surfaces during approach, whereas "jump out" is a sustained attraction during separation. Figure 3A was originally published in Reference [47] © copyright the American Society for Biochemistry and Molecular Biology.

Table 1. Distance controls and their specifications in SFA

Level of control	Type of control	Surface moved	Positional accuracy (Å)	Total range of movement (μm)
Extra fine	Piezoelectric tube	Upper	<1	~1
Fine	Differential spring	Lower	~2	~10
Medium	Differential micrometer	Lower	~500	~200
Coarse	Differential micrometer	Lower	~2000	~2000

with a thin layer of silver (~>50 nm) that acts as opposing semi-mirrors. When the white light passes the two opposing silver coated mica surfaces, the spectrophotometer detects the fringes equal chromatic order (FECO) signal, which is used to calculate the distance (ΔD), by the interference of between reflecting light and transmitting light through the two surfaces. Due to the high accuracy of FECO signal, the distance between the surfaces resolves to less than 1 Å. The two surfaces of the crossed cylinders geometry are precisely approached and withdrawn from one another in the SFA, and the force-distance curves (f-d curves) are generated from the interacting forces. The adhesion force with 1 nN resolution is measured by the distance from the contact of the adhesive surfaces that are attached to each other to their separation, ΔD_{jump}, and the calculation follows this equation.

$$F_{adhesion}=k\times\Delta D_{jump}$$

Essentially, SFA measures the interaction forces between two curved surfaces by the crossed cylinders geometry. Because of their curved surfaces, the measured force can be normalized by the radius of the curved surfaces (R). By using the Derjaguin approximation, the normalized force (F_{curved} (D)/R) is directly transformed into the interaction energy per unit area between the two flat surfaces, which is given by

$$W_{flat}(D)=\frac{F_{curved}(D)}{2\pi\sqrt{R_1R_2}}=\frac{F_{curved}(D)}{2\pi R}$$

$F_{curved}(D)$, $W_{flat}(D)$, R_1 and R_2 are the measured force between two curved surfaces, and the interaction energy per unit area between two flat surfaces, the radius of the curved top surface, and the radius of the curved bottom surface, respectively. Additionally, solvents or vapors can be introduced into the gap between the two surfaces by a capillary force. Thus, the interactions in various media (with different dielectric constants) can be carefully probed. In particular, the introduction of aqueous solutions with different pH and ionic strength enables interaction measurements of biological molecules in conditions similar to the native underwater environments.

1-1-3. Shear Forces Measurement

A new attachment, the bimorph slider, was developed to measure the friction force in complex systems [34]. A motor-driven micrometer generates top surface movement in which the surfaces shear past each other. By using a bimorph slider, which is connected to the piezoelectric equipment, the bottom surface can move in a lateral direction. When the lateral force is placed on the top surface, the strain gauge with a signal conditioning amplifier can evaluate the deflection and send the signal to a computer with data acquisition system. Since the motion of the top surface or the bimorph slider is driven by voltage, which is applied to the motor, the friction device can be calibrated against the weight using the Keyence position detector. The bimorph slider can be used in water because all the wiring connections are coated with appropriate waterproof coating.

1-1-4. Surface Preparations and Hard Wall Distance

The base surface for SFA experiments is mica because mica is naturally flat, optically transparent, and chemically inert. Mica should be cleaved and mounted on the SFA chamber in a dust free-environment before the experiment to prevent surface contamination. To set the offset distance (D=0), both bare mica surfaces are brought into flat contact with air. Then, a sample is evenly and homogeneously mounted onto the bare mica surface by the spin coating of polymer solutions, e-beam deposition of metal/metal oxides, or Langmuir-Blodgett blotting of lipid layer. The actual thickness of the sample film on the mica surface can be monitored by the base of "hard wall" distance (D_{hw}), which is defined as the asymptotic thickness of the compressed film under the increasing normal load [32,33] (Fig. 3). The D_{hw} value can be measured by comparing the offset distance of both bare mica surfaces with the increasing distance of the film-coated surface that is compressed until FECO signal ceases to move to left. Interaction forces between the sample and the mica surfaces are always dependent on the quantity of the sample inbetween the surfaces. Therefore measuring D_{hw} is critical for SFA experiments and it is one of the biggest advantages over AFM, which cannot measure D_{hw}.

2-1. Mussel Adhesive Protein Interactions Mediated by DOPA Chemistry

Mussels strongly adhere to diverse wet surfaces via the flattened adhesive plaque hanging on the end of the byssus matrix, which is a brown bundle of threads. Various mfps have been extracted and investigated as a source of inspiration for the design of underwater coatings and adhesives [25,37-41] (Fig. 4 and Table 2). Although all the mfps have similar basic isoelectric points (pI) at ~9.5, they have variable mass ranging from 5 kDa in mfp-3 to 240 kDa in preCol-D. Another common feature in all the mfps is DOPA, a post-translationally modified tyrosine (Tyr). The DOPA content in each mfp varies from 2 mol% to 30 mol%. In general, the mfps near the adhesion interface have a high proportion of DOPA residue.

DOPA is considered as the key component for underwater adhesion. Contact mechanical tests were introduced for measuring the adhesion properties of DOPA [42,43]. In an important atomic force microscopy (AFM)-based study [44], DOPA was tethered to an AFM cantilever tip and contacted to TiO_2 surfaces in a buffer of pH 7.5. Interestingly, the measured energy was approximately −25 kCal/DOPA, and the interaction renewed reversibly for more than hundred cycles. The reversible bonding between DOPA and metal oxides has been used to improve the capacity of lithium-ion battery [45].

Several AFM tests have been conducted to study the adhesion of mfps in air [46-48]. However, in air, the mfp film behaves as a glassy polymer, in which the mfps may lose their biological properties and important interfacial interactions such as van der Waals

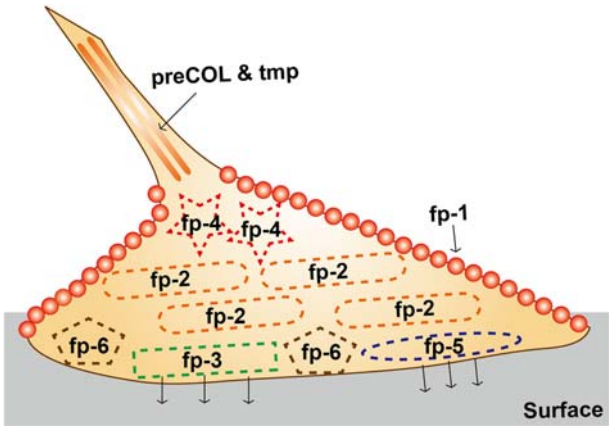

Fig. 4. Mussel foot proteins distribution of known byssal plaque proteins of *Mytilus* species.

Table 2. Work of adhesion for different interactions of mussel foot proteins

Mfp (ref.)	Secondary structure	pH	DOPA (mol%)	Work of adhesion (mJ/m^2)		
				Asymmetric (↔ mica)	Symmetric	
					None	Additive
Mefp-1	PPII	5.5	15	<0.1	<0.1	4.3 (Fe)
Mefp-2	EGF-like	5.5	3	<0.1	<0.1	2.2 (Fe)
Mcfp-3	Random coil	5.5	20	0.3-0.5 (0.4-0.6)	<0.1	1.2 (Mcfp-6)
Mcfp-3	Random coil	3.0	20	1.3-2.0	<0.1	-
Mcfp-4	Unknown	3.0	2	<0.1	<0.1	-
Mefp-5	Random coil	5.5	30	2.3-2.5 (3.0-3.4)	<0.2	-
Mefp-5	Random coil	2.6	30	8-10 (10.5-13.3)	2.5	-
Mefp-6	Unknown	3.0	3	<0.5 (0.66)	0.5	-
Pvfp-1	Unknown	5.5	0	0.2	2.3	-
Pvfp-1	Unknown	3.0	0	1.0	1.6	-
Mefp3 ↔ 5	-	2.6	-	2.3-2.6 (3.0-3.5)	-	
Mefp2 ↔ 5	-	3.0	-	0.9-1.2 (1.2-1.5)	-	

and electrostatic forces, as well as the interdigitation of polymer chain ends [49,50]. However, in water, the protein layer behaves more like a swollen and extended brush, similar to its form under biological conditions. Therefore, the underwater adhesive properties of mfps have been investigated at the molecular level using SFA in wet conditions. Here, we summarize the results of SFA from various literatures (Table 2) and discuss their chemical and biological significance regarding the DOPA content in wet conditions. Because of the tendency of DOPA to be oxidized to dopaquinone, the mfps need to be handled with care. The buffer conditions for all the SFA experiments described below were 0.1 M sodium acetate and 0.25 M KNO_3 at pH 5.5 to maintain the similar ionic strength of seawater (~0.56 M) [23]. KNO_3 was used to replace sodium chloride in the buffer solution to avoid corrosion of the thin silver layers under the mica substrates, which normally have high concentrations of chloride ions and affect the quality of the optical fringes during the SFA experiments. The force-distance curves (f-d curves), adhesion force (F_{ad}), and adhesion energy (W_{ad}) of mfps can be measured by using SFA. The asymmetric mode helps measure the "adhesion" between two different molecules, or between a protein and one type of substrate. In contrast, the symmetric mode measures the "cohesion" of homogeneous molecules.

2-1-1. Asymmetric Mode to Mica

The adhesion between the mfps and mica is summarized in Table 2 (asymmetric mode row). The correlation between the adhesion forces of mfps and their apparent role is discussed on the basis of their amino acid compositions and structures in aqueous solutions. The adhesion forces have been measured in the following manner. One surface is coated with each mono-layered mfp film, while the other surface is mica itself. Mfp-1, 2, 3, 5, and 6 achieved cohesion forces of ~0.1, ~0.1, ~2.6, ~1.7, and ~0.5 mJ/m^2, respectively [25, 37-41].

Both mfp-2 and mfp-6 are dominant in the adhesive plaque of byssus matrix; however, they exhibit negligible adhesion force to mica, probably owing to their low DOPA content [51,52]. Interestingly, mfp-1 is unable to provide strong adhesion force even after a prolonged contact time or an increased load, despite the 10-15 mol% concentration of DOPA in 0.1 M sodium acetate, 0.25 M KNO_3 buffer at pH 5.5 [39]. This is probably because of the effect of its relatively stiff secondary structure. Mfp-1, which is delocalized in the thin coating of byssus matrix, is mainly composed of 60 to 80 degenerate repeats of a stiff decapeptide (AKPSYPPTYK) sequence with polyproline type II helix. In general, a stiff structure in adhesive polymers reduces their adhesion to most adherents. On the other hand, mfp-3 and mfp-5 are found at the interface between the marine substratum and the mussel adhesive plaque [40,51,53], and they are likely to exhibit a flexible random coil conformation in water, thus making themselves adaptable to diverse surface textures and chemistries. Indeed, the adhesion of mfp-3 and mfp-5 to mica is more than enough to hold the weight of the mussel (~100 g·m) by hydrogen bonds and coordination interactions between the DOPA and mica. Thus, mfp-3 and mfp-5 act as interfacial adhesives. In another SFA study, the interaction strengths of mfps to other substrates such as polystyrene (PS), poly(methyl methacrylate), SiO_2, and TiO_2 generally showed a similar trend as those of mfps to mica [23]. Collectively, all the asymmetric results support the expected function of mfps in correlation to their distribution in the plaque, i.e., mfp-1 acts as the "protective" coating while mfp-3 and mfp-5 act as the "interfacial glue" to bind to the surface (Fig. 4).

2-1-2. Symmetric Mode

Second, the attraction forces between mfps (cohesion of mfp) are also summarized in Table 2 (symmetric mode row). We also discuss the interrelation between their cohesiveness and the biological significance based on the DOPA-meditated chemistry. The metal-ion-mediated cohesions of mfps are measured because mfps use strong and reversible coordinative interactions between metal ions and DOPA. The results are summarized in Table 2.

A byssal cuticle is one of the toughest biomaterials providing stiffness (E_i=~1.7 GPa) comparable to that of a conventional epoxy resin, and extensibility (δ=~100%) comparable to that of rubber [54]. However, mfp-1, the only known protein in the byssal cuticle, showed no more than 0.1 mJ/m^2 of cohesion force in the buffer consisting of 0.1 M sodium acetate and 0.25 M KNO_3 at pH 5.5-8.2 [39]. This result indicates that the cohesive interactions between

the two opposing mfp-1 films require assistance from other molecules in the byssal cuticle. Elemental analysis of the byssus matrix revealed that *Mytilus* byssus has 10^6 times higher Fe than standard seawater, while the elemental maps of the cross-section, generated by secondary ion mass spectroscopy (SIMS), revealed that Fe is delocalized only in the cuticle. Confocal Raman microscopy confirmed the presence of Fe^{3+}-DOPA complexes in the cuticle. Therefore, the effects of Fe^{3+}-DOPA complexes on the mechanical properties of the only known byssal cuticle protein, mfp-1, were investigated using SFA. Surprisingly, the cohesion of mfp-1 dramatically increased in the presence of Fe^{3+} ions and reached the maximum value, ~4.3 mJ/m^2, at the optimal iron concentration of 10 μM. Presumably, the formation of bis- and tris-DOPA-Fe^{3+} complexes is responsible for the cohesion. The Fe^{3+}-mediated bridging between two opposing mfp-1 films was fully reversible and reproducible in pH 5.5 buffer for more than ten cycles. The results indicate that Fe^{3+}-DOPA-complex-mediated mfp-1 crosslinking is one of the contributors to the unusual toughness of *Mytilus* byssal coating [16]. The cohesion of mfp-1 disappeared at a higher concentration of Fe^{3+} (~100 μM), probably because of the formation of a nonbridging mono-Fe^{3+}-DOPA complex. Because Fe^{3+} ion has a redox activity, Fe^{3+} ion in the mussel cuticle also forms covalent crosslinks between DOPA residues.

Mfp-2 is the major protein in the mussel adhesive plaque in which the underwater adhesion between byssus matrix and substratum actually occurs. Mfp-2 has one calcium-binding motif and 3 mol% DOPA. Similar to mfp-1, no detectable cohesion between two opposing mfp-2 films was observed in the SFA system; however, the addition of metal ions (Ca^{2+} and Fe^{3+} ions) to the aqueous medium induced cohesion between the two opposing mfp-2 films in the aqueous buffers. Weak and reversible underwater cohesion was detected in the presence of Ca^{2+} ions (0.3 mJ/m^2), whereas strong and reversible cohesion was detected in the presence of Fe^{3+} ions (~2.2 mJ/m^2), despite the low DOPA content (<3 mol%) [51]. The results indicate that the metal-dependent cohesive interactions of mfp-2 play a key role in the mussel adhesive plaque.

2-1-3. Protein-protein Interaction (Asymmetric Mode)

As a major protein in the adhesive plaque, mfp-2 should interact with other mfps in the mussel adhesive plaque (i.e., mfp-1, mfp-3, mfp-5, and mfp-6) [51]. No detectable adhesion between mfp-1 and mfp-2 was observed even in the presence of Fe^{3+} ions, indicating no direct interaction between a coating protein (mfp-1) and a bulk adhesive protein (mfp-2). The interaction between mfp-2 (a bulk adhesive protein) and mfp-3/mfp-5 (an interfacial adhesive protein) was also measured. Mfp-2 film strongly, reversibly, and immediately adhered to mfp-5 film (W_{ad} ~1.3 mJ/m^2). On the other hand, the adhesion between mfp-2 and mfp-3 (W_{ad} ~1.0 mJ/m^2) was slightly unclear and not instantaneous, because mfp-2 film seemed to be displaced by the mfp-3 of the opposite side during the SFA experiments, probably because of the difference in their molecular weights. As expected from the DOPA content, mfp-5 showed stronger adhesion to mica than to mfp-3. No adhesion enhancement was observed on Fe^{3+} addition in the mfp-2-, mfp-3-, and mfp-5-binding experiments, indicating that no Fe^{3+}-DOPA complex formed between mfp-2 and the interfacial adhesive proteins (mfp-3 and mfp-5).

DOPA has a tendency to oxidize to dopaquinone, thereby easily losing the adhesion ability when exposed to air or seawater. Therefore, the introduction of antioxidant molecules is required for a successful underwater adhesion. Indeed, an antioxidant protein is present in the adhesive plaque. Mfp-6 contains a thiol group with antioxidant property. When mfp-6 was added into the medium between the oxidized mfp-3 film and mica surfaces, where previously no adhesion had occurred because of DOPA oxidation, there was nearly 100% recovery of the initial adhesion [52]. After carboxymethylation of the thiols, mfp-6 failed to restore mfp-3 cohesion from the oxidation. This indicates that the thiol groups in mfp-6 presumably restore DOPA from dopaquinone.

2-2. Cation-π Interaction

Cation-π interaction is the strongest noncovalent interaction in the aqueous environment because of the low desolvation penalty of the aromatic group in a water molecule [22]. Cation-π interactions exist between an electron-rich π system (e.g., Phe, Tyr, and Trp) and monovalent alkali metal ions (e.g., Li^+, Na^+, and K^+) or positively charged molecules (e.g., NH_4^+, His, Lys, Arg). Recently, systematic and simplified experiments have been performed to unravel the contribution of cation-π interactions in underwater adhesion. Herein, we summarize four studies to understand the cation-π interactions in wet adhesion and discuss the interrelation between the nature of cation-π interactions and their biochemistry (Fig. 5).

2-2-1. Pvfp-1

Intriguingly, pvfp-1, a coating protein from the Asian green mus-

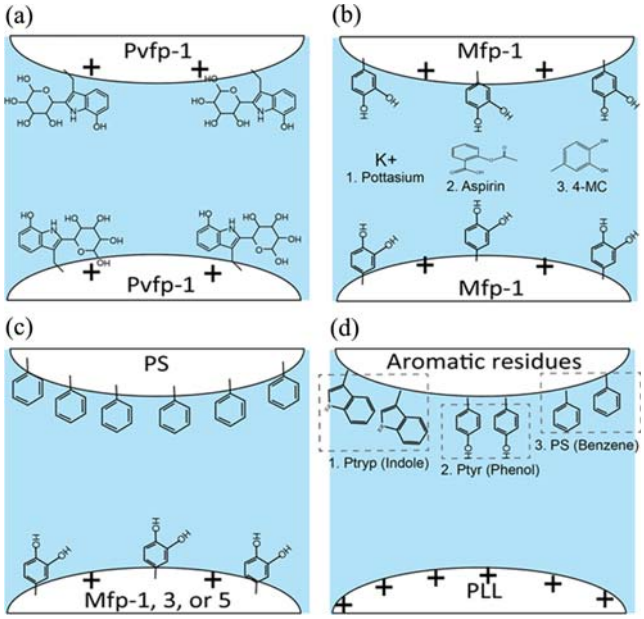

Fig. 5. Illustration of four types of the SFA experimental setups for understanding the cation-π interaction in underwater adhesion. (a) Symmetric mode between the two opposing pvfp-1 films. (b) Symmetric mode between the two opposing mfp-1 films and the effects from the addition of potassium, aspirin or 4-methyl catechol (4-MC) into medium. (c) Asymmetric mode between polystyrene (PS) coated surfaces and three different mfps (mfp-1, mfp-3, or mfp-5). (d) Asymmetric mode experiments between a positively charged polymer (PLL) and three different aromatic groups-containing polymers: poly-L-tryptophan (PTrp) with indole group, poly-L-tyrosine (PTyr) with phenol group, or PS with benzene group.

sel (*Perna viridis*), adheres to the surface without the use of DOPA-meditated chemistry [24]. The biochemistry and molecular biology of pvfp-1 reveal that a tandem repetition of the decapeptide in the coating protein is preserved; however, the DOPA residue is completely replaced by C^2-mannosyl-7-hydroxytryptophan (Man7OHTrp) in pvfp-1. Unlike mfp-1, interestingly, an SFA test on symmetric pvfp-1 films showed 2.3 mJ/m^2 of significant cohesion force, despite the lack of DOPA, in 0.1 M sodium acetate and 0.25 M KNO_3 buffer at a pH of 5.5. Moreover, the oxidation of Man7OHTrp did not reduce the adhesion or cohesion. The cation-π interactions between Man7OHTrp and lysyl side chains are expected as the key factor for the strong adhesion between the pvfp-1 monomolecular films. It is unknown why the replacement of DOPA with Man7OHTrp induced huge adhesion in pvfp-1. Presumably, the indole group of Man7OHTrp, with a higher electron density in pvfp-1 than that in the catechol group of DOPA residue in mfp-1, enhanced the cation-π interactions in the same buffer, leading to a strong cohesion [21,55, 56]. Then, an inevitable question arises as to why there is no adhesion between the two opposing mfp-1 films.

2-2-2. Mfp-1/Mfp-1 Interaction at a Low Potassium Ion (K^+) Concentration

To answer the above question, symmetric SFA experiments with mfp-1 at different pH and K^+ ion concentrations in the testing buffer were conducted to monitor the changes in the cohesion of mfp-1 [25]. Mfp-1 is composed of ~20 mol% of positively charged amino acids (mainly lysine (Lys)) and ~20 mol% of aromatic amino acids (mainly DOPA and Tyr), but no negatively charged amino acid. There was no change in the cohesion between the two opposing mfp-1 films with the variation of pH (from 3.0 to 5.5); however, the cohesion was strongly affected by the changes in K^+ ion concentration in the buffer. The cohesion of mfp-1 gradually decreased with increasing K^+ ion concentration. Because K^+ ion has binding energy similar to that of DOPA or Tyr, as with positively charged Lys residue, DOPA-Lys or Tyr-Lys crosslinks in the two opposing mfp-1 films gradually decreased with increasing K^+ ion concentration in the buffer system. To clarify the presence of the cation-π interactions in this system, the effects of small aromatic compounds on the cohesion of mcfp-1 films were investigated. The addition of small aromatic groups with different electron densities in the π group (aspirin and 4-methylcatechol (4-MC)) into the medium improved the cohesion of mfp-1 by up to ~2.3 mJ/m^2 and ~3.6 mJ/m^2. 4-MC, which has a higher electron density (in the phenyl group) than that of aspirin, induced a stronger cohesion between the mfp-1 films [25]. One possible explanation for this improvement is that both aspirin and 4-MC bridged the mcfp-1 film surfaces, because the face of a single aromatic molecule can couple two different cation species.

2-2-3. Mfp Interactions with Polystyrene

To clarify the contribution of cation-π interactions in underwater adhesion of mussel, a simplified SFA experiment was performed: One surface was coated with PS, an aromatic polymer with benzene pendant groups, and the other surface was coated with mfp-1, mfp-3, or mfp-5 [23]. Mfp-1, mfp-3, and mfp-5 showed 0.33, 2.69, and 2.37 mJ/m^2 of adhesive force to mica, respectively. In the experiments, the hydrophobic interactions, cation-π interactions, and π-π stacking were considered as the important interaction mechanisms, while the hydrogen bond, catechol-meditated coupling, and electrostatic bond contributed less to the adhesion. Mfp-1, mfp-3, and mfp-5 contain 28.6, 35.5, and 29.1 mol% of hydrophobic side-chains (A, I, V, L, M, F, Y, and W), respectively. In the same order, they contain 20.4, 24.5, and 22.6 mol% of positively charged side chains (H, R, and K), respectively, and 19.2, 26.5, 26.2 mol% of aromatic side chains (Y, R, W, and F), respectively. Overall, the amino acid content that forms the cation-π, π-π stacking, and hydrophobic interactions increased in the order of mfp-3, mfp-5, and mfp-1. As expected from the order of the amino acid content, the actual adhesion of mfps increased in the order of mfp-3, mfp-5, and mfp-1. For the adhesion of mfps to mica, which has a rocky surface, mfp-3 showed a weaker adhesive force than mfp-5 because of its lower DOPA content. However, in the adhesion of mfps to PS, mfp-3 achieved the strongest adhesion to PS, probably because of the higher cation and hydrophobic residue concentrations, thus achieving cation-π interactions, π-π stacking, and hydrophobic interactions.

2-2-4. Homopolymer Systems

To address the contribution of cation-π interactions only in underwater adhesion, model systems were designed to understand the mechanical nature of cation-π interactions in aqueous solution, with the exclusion of π-π stacking and salt bridge [55]. One surface was coated with positively charged poly-L-lysine (PLL) (primary amine, NH_3R^+), and the other surface was coated with one of the three homopolymers with π electron-possessing side groups—poly-L-tryptophan (PTrp), poly-L-tyrosine (PTyr), and PS. The adhesive forces between the three different aromatic polymer films and PLL at pH 3 were ~1.9 mJ/m^2 (PTrp), ~1.6 mJ/m^2 (PS), and ~0.8 mJ/m^2 (PTyr). The order of adhesive strength is in good accordance with the quadruple strength in the order of indole>benzene>phenol [22,55,56]. Interestingly, the adhesion value between PTrp and PLL films is comparable to Fe^{3+}-DOPA chelation and is much stronger than the salt-bridge energy between the two oppositely charged electrolyte multilayer of PLL and poly-L-glutamic acid (PGA) in aqueous solution, as previously measured using SFA. To investigate the effect of the competing cation (K^+) on these cation-π interactions, the adhesion between PTrp and PLL was measured using varying KNO_3 concentrations in the aqueous buffer. By increasing the KNO_3 concentration from 0 to 0.2 M, the adhesion between PTrp and PLL decreased from ~2.0 to ~0.36 mJ/m^2 at pH 3. This is most probably because the increased K^+ ions formed an electrical double layer on the PLL surface and competitively bound to the indole groups on the PTrp surface instead of the ammonium groups of PLL. To investigate the effect of this type of competing cation, the adhesion between PTrp and PLL was measured in a medium buffer with four different cations (Li^+, Na^+, K^+, and NH_4^+). The addition of cation decreased the adhesion force in the aqueous solution more effectively, as the hydration radius of cation increases in the order of NH_4^+/K^+>Na^+>Li^+. This indicates that the "binding" strength of the hydrated cations to PTrp follows the order of NH_4^+/K^+>Na^+>Li^+, same as the hydration radius. This result well explains that the cation-π interactions are inversely proportional not to the naked radius but to the hydration radius of the cation, because a larger hydration shell blocks the cation-π interactions more effectively. To better understand the cation-π interactions in biological phenomena, two different quaternary ammonium cations, NR_4^+, the potassium channel blocker (triethylammonium, TEA, $(CH_3CH_2)_4N^+$), and the neurotransmitter (acetylcholine, Ach, $(CH_3)3(CH_3COOCH_2CH_2)N^+$), were added

into the medium buffer to compete with the interactions between PTrp and PLL. The addition of a trace amount of TEA or Ach (<0.5 mM) dramatically decreased the adhesion between PTrp and PLL (Fig. 5(c)), which was a more significant decrease than that from the addition of the same concentrations of NH_4^+ or K^+ ions. This is probably because of the quaternary ammonium ion that binds to the aromatic groups with a higher affinity than K^+ ion does, indicating a "binding" order of NR_4^+>NH_3R^+>NH_4^+~K^+ to PTrp under physiological conditions. Thus, the results well explain that potassium channel blockers and neurotransmitters bind effectively to aromatic residues even in the presence of NH_4^+, K^+, and Na^+ ions in physiological conditions [56].

2-3. Complex Coacervate

The last key contributor for underwater adhesion investigated by SFA was the complex coacervate. Sandcastle worm (Fig. 1(d)) builds sandcastles on marine substrata by connecting sand particles with its specialized underwater adhesive protein mixture [29]. It has been expected that marine sandcastle worms use the complex coacervation process to condense their adhesive proteins in the aqueous environment. Complex coacervation is a fluid/fluid phase separation that occurs when two or more oppositely charged polyelectrolytes are mixed in an aqueous solution at a certain pH and ionic concentration. The oppositely charged polyelectrolytes neutralize each other and are condensed into a dynamic round-shaped fluid droplet within a polyelectrolyte-depleted fluid. The polyelectrolyte condensed phase is called the complex coacervate.

The coacervates have great potential for application in coating and adhesive materials outside and within the biomedical material field owing to their unique properties—no diffusion of protein into water, low-interfacial energy in aqueous media, and super high protein concentration (approximately, >1,000 mg/mL) [43,57]. The mechanical and interfacial properties of coacervate phases have been studied by SFA to define the nature of the complex coacervates (Fig. 6). First, a study of the interfacial energy (γ) measurement of the complex coacervate with a recombinant mussel adhesive protein (fp-151) was conducted, and the process was briefly described as follows. An aqueous mixture of oppositely charged electrolytes (fp-151 and hyaluronic acid) was added into the gap between the two mica surfaces [58]. Upon reaching an equilibrium, they evolved into two bulk phases: a dense coacervate phase and a dilute polymer-deficient aqueous phase. A meniscus of the coacervate phase formed a bridge between the two mica surfaces, producing a capillary adhesion during the separation of the two surfaces. The γ at the aqueous/coacervate phase interface was determined from this adhesion force. Consequently, the γ value of this model system was revealed to be very low, <3 mJ/m^2, enabling the coacervate to readily deliver valuable materials into microholes. Second, as an effort to define how the adhesives from marine organisms are secreted as coacervate flows through a narrow secreting vessel from the gland to the outside, the dynamic viscosity and friction coefficient of coacervates with different mixing ratios of the oppositely charged polyelectrolytes were measured using SFA. As the model system, a mussel-inspired coacervate was prepared by mixing a recombinant mussel adhesive protein (fp-151) with hyaluronic acid (HA). The coacervate at the optimal ratio (neutral net-charge state) shows shear-thinning behavior, while at the other ratios, it shows shear-thickening behavior. This result enabled us to propose a hypothesis about the charge balance state of adhesive coacervation during its secretion [54]. When an adhesive is secreted through a vessel of very narrow diameter (d=20-30 μm), it lies under a high shear rate (γ, $\gamma \propto d^{-1}$). Thus, the optimal coacervate would improve its flow through the vessel, whereas the charge-unbalanced coacervate mixtures would

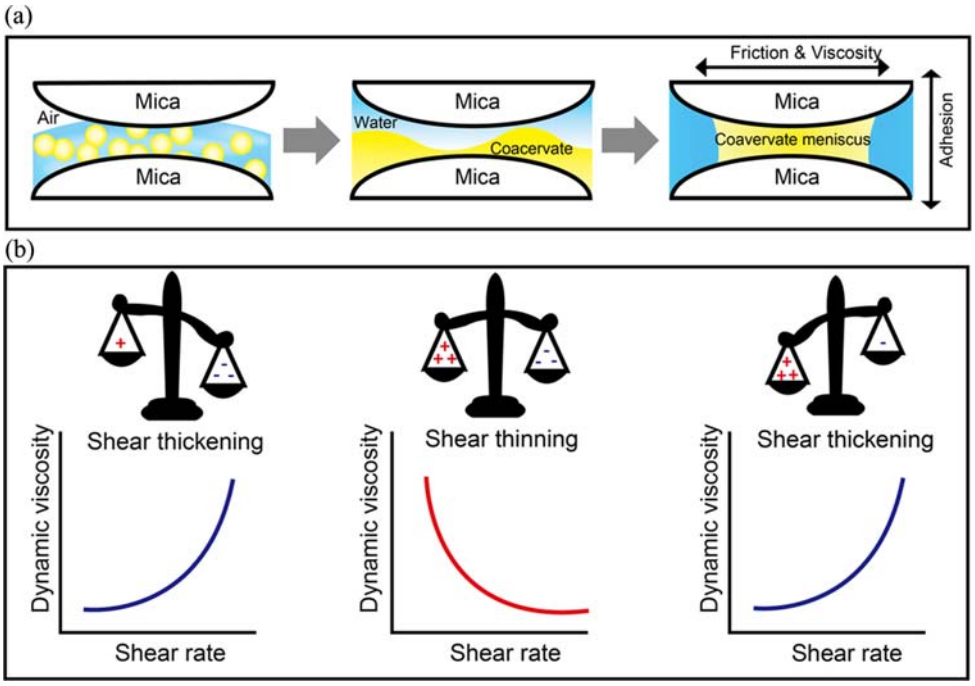

Fig. 6. (a) Schematic of the SFA experimental procedure to measure the viscoelastic properties of the coacervate of hyaluronic acid (HA, a negatively charged polymer) and recombinant mussel adhesive protein (fp-151-RGD, a positively charged polymer). (b) Viscosity-shear rate profiles of coacervates that depend on the mixing ratio of HA and fp-151-RGD.

effectively clog the vessel due to shear thickening. The coacervates have high friction coefficient regardless of the mixing ratio, thus preventing the slippage of the foot-to-surface contact in mussels. This result well explains the phenomenal observation that mussels bear their weight with no sign of slippage when the mussel-attached object is lifted outside of water.

CONCLUSIONS

Surface forces apparatus (SFA) is an ideal nanomechanical tool to measure interactions of molecules in aqueous environments. The underwater adhesion mechanisms of marine fouling organisms have been explored by SFA techniques in several studies, and three key mechanisms for successful underwater adhesion, i.e. DOPA chemistry, cation-π interactions and complex coacervation, have been suggested to date. SFA techniques have not yet fully elucidated all the mechanisms of the marine fouling organisms-produced adhesives, but the three key mechanisms that marine fouling organisms have exploited for survival should be effective strategies for the development of underwater adhesive for biomedical applications.

ACKNOWLEDGEMENTS

This work was supported by the Marine Biomaterials Research Center under Marine Biotechnology Program, Ministry of Oceans and Fisheries Affairs, Korea. We also acknowledge the National Research Foundation of Korea Grant funded by the Ministry of Science, ICT and Future Planning (MSIP) (NRF-C1ABA001-2011-0029960 & NRF-2013- Fostering Core Leaders of the Future Basic Science Program).

REFERENCES

1. A. Pizzi and K. L. Mittal, *Handbook of adhesive technology, revised and expanded*, CRC Press, New York (2003).
2. S. R. White, N. Sottos, P. Geubelle, J. Moore, M. R. Kessler, S. Sriram, E. Brown and S. Viswanathan, *Nature*, **409**, 794 (2001).
3. J.-Y. Kim, J.-H. Yoon, D.-H. Kim and S.-B. Kim, *Korean J. Chem. Eng.*, **29**, 503 (2012).
4. C.-C. Chu, J. A. Von Fraunhofer and H. P. Greisler, *Wound closure biomaterials and devices*, CRC Press (1996).
5. W. D. Spotnitz and S. Burks, *Transfusion*, **48**, 1502 (2008).
6. C. D. Amsler, *Algal chemical ecology*, Springer, Heidelberg (2008).
7. C. J. Kavanagh, M. P. Schultz, G. W. Swain, J. Stein, K. Truby and C. D. Wood, *Biofouling*, **17**, 155 (2001).
8. Y. Sun, S. Guo, G. C. Walker, C. J. Kavanagh and G. W. Swain, *Biofouling*, **20**, 279 (2004).
9. D. S. Hwang, A. Masic, E. Prajatelistia, M. Iordachescu and J. Herbert Waite, *Acta Biomater.*, **9**, 8110 (2013).
10. L. A. Thomas and C. O. Hermans, *Biol. Bull.*, **169**, 675 (1985).
11. L. Joll, *Mar. Biol.*, **36**, 327 (1976).
12. J. A. Callow and A. M. Smith, *Biological Adhesives*, Springer, Berlin (2006).
13. J. H. Waite, *Integr. Comp. Biol.*, **42**, 1172 (2002).
14. H. Zeng, *Polymer Adhesion, Friction, and Lubrication*, Wiley, New Jersey (2012).
15. Y. J. Yang, Y. S. Choi, D. Jung and H. J. Cha, *Korean J. Chem. Eng.*, **28**, 1744 (2011).
16. H. Zeng, D. S. Hwang, J. N. Israelachvili and J. H. Waite, *Proc. Natl. Acad. Sci.*, **107**, 12850 (2010).
17. L. A. Burzio and J. H. Waite, *Biochemistry*, **39**, 11147 (2000).
18. S. W. Taylor, D. B. Chase, M. H. Emptage, M. J. Nelson and J. H. Waite, *Inorg. Chem.*, **35**, 7572 (1996).
19. J. H. Waite, *Comp. Biochem. Phys. B*, **97**, 19 (1990).
20. D. A. Dougherty, *Science*, **271**, 163 (1996).
21. S. Mecozzi, A. P. West and D. A. Dougherty, *Proc. Natl. Acad. Sci.*, **93**, 10566 (1996).
22. J. P. Gallivan and D. A. Dougherty, *J. Am. Chem. Soc.*, **122**, 870 (2000).
23. Q. Lu, E. Danner, J. H. Waite, J. N. Israelachvili, H. Zeng and D. S. Hwang, *J. R. Soc. Interface*, **10**, 20120759 (2013).
24. D. S. Hwang, H. Zeng, Q. Lu, J. Israelachvili and J. H. Waite, *Soft Matter*, **8**, 5640 (2012).
25. Q. Lu, D. S. Hwang, Y. Liu and H. Zeng, *Biomaterials*, **33**, 1903 (2012).
26. D. S. Hwang, J. H. Waite and M. Tirrell, *Biomaterials*, **31**, 1080 (2010).
27. J. H. Waite, N. H. Andersen, S. Jewhurst and C. Sun, *J. Adhes.*, **81**, 297 (2005).
28. A. Srivastava, J. H. Waite, G. D. Stucky and A. Mikhailovsky, *Macromolecules*, **42**, 2168 (2009).
29. H. Zhao, C. Sun, R. J. Stewart and J. H. Waite, *J. Biol. Chem.*, **280**, 42938 (2005).
30. J. Israelachvili, Y. Min, M. Akbulut, A. Alig, G. Carver, W. Greene, K. Kristiansen, E. Meyer, N. Pesika and K. Rosenberg, *Rep. Prog. Phys.*, **73**, 036601 (2010).
31. T. Hugel and M. Seitz, *Macromol. Rapid Commun.*, **22**, 989 (2001).
32. A. Engel and D. J. Müller, *Nat. Struct. Mol. Biol.*, **7**, 715 (2000).
33. M. Benz, T. Gutsmann, N. Chen, R. Tadmor and J. Israelachvili, *Biophys. J.*, **86**, 870 (2004).
34. Y. Min, M. Akbulut, J. R. Sangoro, F. Kremer, R. K. Prud'homme and J. Israelachvili, *J. Phys. Chem.*, **113**, 16445 (2009).
35. J. Israelachvili and R. Pashley, *Nature*, **300**, 341 (1982).
36. B. Bhushan, J. N. Israelachvili and U. Landman, *Nature*, **374**, 607 (1995).
37. T. H. Anderson, J. Yu, A. Estrada, M. U. Hammer, J. H. Waite and J. N. Israelachvili, *Adv. Funct. Mater.*, **20**, 4196 (2010).
38. D. S. Hwang, M. J. Harrington, Q. Lu, A. Masic, H. Zeng and J. H. Waite, *J. Mater. Chem.*, **22**, 15530 (2012).
39. Q. Lin, D. Gourdon, C. Sun, N. Holten-Andersen, T. H. Anderson, J. H. Waite and J. N. Israelachvili, *Proc. Natl. Acad. Sci.*, **104**, 3782 (2007).
40. J. Yu, W. Wei, E. Danner, J. N. Israelachvili and J. H. Waite, *Adv. Mater.*, **23**, 2362 (2011).
41. J. Yu, W. Wei, M. S. Menyo, A. Masic, J. H. Waite and J. N. Israelachvili, *Biomacromolecules*, **14**, 1072 (2013).
42. B. P. Lee, C. Y. Chao, F. N. Nunalee, E. Motan, K. R. Shull and P. B. Messersmith, *Macromolecules*, **39**, 1740 (2006).
43. M. Guvendiren, P. B. Messersmith and K. R. Shull, *Biomacromolecules*, **9**, 122 (2007).
44. H. Lee, N. F. Scherer and P. B. Messersmith, *Proc. Natl. Acad. Sci.*, **103**, 12999 (2006).
45. M. H. Ryou, J. Kim, I. Lee, S. Kim, Y. K. Jeong, S. Hong, and J. W. Choi, *Adv. Mater.*, **25**, 1570 (2013).

46. D. S. Hwang, H. J. Yoo, J. H. Jun, W. K. Moon and H. J. Cha, *Appl. Environ. Microbiol*., **70**, 3352 (2004).
47. D. S. Hwang, Y. Gim and H. J. Cha, *Biotechnol. Prog*., **21**, 965 (2005).
48. D. S. Hwang, Y. Gim, H. J. Yoo and H. J. Cha, *Biomaterials*, **28**, 3560 (2007).
49. N. Maeda, N. Chen, M. Tirrell and J. N. Israelachvili, *Science*, **297**, 379 (2002).
50. C. Creton, *MRS Bull*., **28**, 434 (2003).
51. D. S. Hwang, H. Zeng, A. Masic, M. J. Harrington, J. N. Israelachvili and J. H. Waite, *J. Biol. Chem*., **285**, 25850 (2010).
52. J. Yu, W. Wei, E. Danner, R. K. Ashley, J. N. Israelachvili and J. H. Waite, *Nat. Chem. Biol*., **7**, 588 (2011).
53. E. W. Danner, Y. Kan, M. U. Hammer, J. N. Israelachvili and J. H. Waite, *Biochemistry*, **51**, 6511 (2012).
54. N. Holten-Andersen, G. E. Fantner, S. Hohlbauch, J. H. Waite and F. W. Zok, *Nat. Mater*., **6**, 669 (2007).
55. Q. Lu, D. X. Oh, Y. Lee, Y. Jho, D. S. Hwang and H. Zeng, *Angew. Chem. Int. Ed*., **125**, 4036 (2013).
56. S. E. Wheeler and K. Houk, *J. Am. Chem. Soc*., **131**, 3126 (2009).
57. D. Priftis, R. Farina and M. Tirrell, *Langmuir*, **28**, 8721 (2012).
58. D. S. Hwang, H. Zeng, A. Srivastava, D. V. Krogstad, M. Tirrell, J. N. Israelachvili and J. H. Waite, *Soft Matter*, **6**, 3232 (2010).